Microscopic force driving the photoinduced ultrafast phase transition: Time-dependent density functional theory simulations of $IrTe_2$

Wen-Hao Liu,[1,2] Jun-Wei Luo,[1,2,3,*] Shu-Shen Li,[1,2,3] and Lin-Wang Wang[4,†]

[1]*State Key Laboratory of Superlattices and Microstructures, Institute of Semiconductors, Chinese Academy of Sciences, Beijing 100083, China*

[2]*Center of Materials Science and Optoelectronics Engineering, University of Chinese Academy of Sciences, Beijing 100049, China*

[3]*Beijing Academy of Quantum Information Sciences, Beijing 100193, China*

[4]*Materials Science Division, Lawrence Berkeley National Laboratory, Berkeley, California 94720, USA*

Photoinduced phase transitions can have complex and intriguing behaviors more than material ground-state dynamics. Understanding the underlying mechanism can help us to design new ways to manipulate the materials. A variety of mechanisms has been proposed to explain the photoinduced phase transitions of $IrTe_2$, but a consensus has yet to be reached. Here, we study the photo-induced phase transitions of $IrTe_2$ by performing the real-time time-dependent density functional theory (rt-TDDFT) simulations in combination with the occupation constrained DFT method. We reveal that the microscopic driving force for the photo-induced phase transitions arises from the tendency to lower the energy levels occupied by the excited carriers, through the increase or decrease of the associated atomic pair distances, depending on whether the newly occupied states are antibonding or bonding states, respectively. The geometric constraints between different bonds represented by the Poisson ratio can bring together different tendencies from different atomic pairs, thus forming a complex intriguing dynamic picture depending on the intensity of the excitation. We also find that phonons don't play a primary role, but can assist the phase transition. These findings imply that one can control the structural phase transitions by selectively exciting photocarriers into designated atomic states using appropriate photon sources.

I. INTRODUCTION

The manipulations of spin, charge, orbital, and lattice degrees of freedom in materials have been used to produce a variety of astonishing phenomena and functionalities, from high-temperature superconductivity to emergent particles with fractional charge [1–7]. The interweaving of these degrees of freedom in materials forms the basis for many exciting fields related to cooperative material phenomena. However, it also presents a challenge to disentangle these interactions, to elucidate their individual roles. In addition to conventional means such as changes of temperature and pressure, photoexcitation has recently been used to control the structural phase transitions in solids in an ultrafast time scale. For instance, the photoexcitation induces charge density wave (CDW) transitions in transition-metal dichalcogenides (TMDCs) on an unparalleled time scale (several hundreds of femtoseconds), near the limit of atomic motions [8–12].

Unlike general TMDCs where the well-known CDW transition results in opening an energy gap at the Fermi level E_f, $IrTe_2$ is special because it preserves its metallic properties in both high-temperature (HT) hexagonal crystal phase and low-temperature (LT) triclinic crystal phase [13,14]. Both x-ray-diffraction measurements and density functional theory (DFT) calculations reveal that the electronic structure of $IrTe_2$ near E_f primarily arises from Ir $5d$ and Te $5p$ orbitals [14–17]. A variety of mechanisms have been proposed to explain the structural phase transition between these two crystal phases. In earlier studies, mechanisms based on collective degrees of freedom have been proposed as the main force for the phase transition, such as the charge-orbital density wave [18] or orbital-driven Peierls instability [19]. However, recent experimental and theoretical works also illustrate that it is the Te p orbital, rather than the CDW, playing the main role in causing a local bonding instability in the observed structural phase transition [17,20,21]. The d_{xy} orbital of the Ir-Ir dimers is also suggested to play a dominant role in the structural phase transition [14,16,22,23]. An interplay among the charge-density-wave-like lattice modulation, in-plane dimer ordering, and the uniform lattice deformation is also postulated as the origin of phase transition [16]. However, most of the above discussions are for thermal dynamic induced phase transitions. Very recently, Ideta *et al.* [23] conducted the photoexcitation induced phase transition in $IrTe_2$, and suggested the association of the phase transition to the electron filling of the high-lying empty antibonding bands. However, it is unclear why the occupation of empty antibonding bands will drive the phase transition, and the microscopic origin underlying the photoinduced phase transition in $IrTe_2$ is still under intensive debate. Most of the above studies are based on experimental observations, together with qualitative arguments or simple DFT calculations. Unable to turn on and off different interactions in the experiment makes it difficult to analyze the roles of different mechanisms. That gap can be filled by theoretical simulations.

*jwluo@semi.ac.cn

†lwwang@lbl.gov

In this paper, we attempt to unravel the microscopic force driving the structural phase transition under photoexcitation by using $IrTe_2$ as a model system through performing rt-TDDFT simulations in combination with occupation constrained DFT calculations [24,25]. This combination allows the access to the microscopic forces and mechanisms which drive the structural transition, and offers the possibility of disentangling interactions among different degrees of freedom. Our rt-TDDFT simulation reproduces the experimentally observed structural transition in $IrTe_2$ under irradiation of a laser pulse. We uncover that the fundamental microscopic force driving the structural transition originates from the energy gain through lowering the energy levels of the Ir-Ir dimer antibonding bands occupied by the photoexcited electrons. This results in a force to dissociate the Ir-Ir dimers. We also demonstrate that additional photoelectrons excited by a stronger laser intensity occupy the bonding bands of interlayer Te-Te bonds, yielding an unexpected transition to a different metastable structure. These findings shed light on photoinduced phase transitions in solids, and reveal general principles which can be applied to many different laser pulses induced structural phase transitions, usually from lower symmetry phases to higher symmetry phases.

II. RESULTS

$IrTe_2$ stabilizes in a CdI_2-type hexagonal structure ($P\bar{3}m1$) at HT and undergoes a structural transition to a triclinic structure ($P\bar{1}$) below temperature $T_S \approx 280$ K [15,17,26]. The LT structure possesses a CDW together with a lattice modulation at a wave vector $q_{1/5}(1/5,\ 0,\ 1/5)$ [16,26]. Figures 1(a) and 1(b) show that, different from the HT phase where the covalently bonded Ir-Ir pairs have the same bond length of 3.9 Å, the LT phase exhibits a periodic lattice distortion in a lattice modulation at $q_{1/5} = (1/5, 0, 1/5)$ as a result of the dimerization of every third Ir-Ir pair in a shorter bond length of 3.07 Å. By performing ground-state *ab initio* molecular dynamics (AIMD) simulation at temperature $T = 200$ K, we obtain the initial system of $IrTe_2$ in a 120-atom supercell, which is a structure containing eight Ir-Ir dimers with a bond length (3.070 Å) 22–24% shorter than the remaining Ir-Ir nondimers with bond length of 3.942–4.054 Å, in excellent agreement with experimental data of the LT structure [13,14]. Based on this structure, we then utilize the rt-TDDFT approach to simulate the time evolution of $IrTe_2$ under irradiation of a laser pulse. The simulated laser pulse has an electric field $E(t) = E_0\cos(\omega t)\exp[-(t-t_0)^2/(2\sigma^2)]$, where E_0 is the amplitude of the electric field, $t_0 = 60$ fs, the pulse width $2\sigma = 25$ fs, and the photon energy $\hbar\omega = 3.1$ eV, which represents the 400-nm optical pump pulse used in experiment [23].

Figure 1(d) shows the rt-TDDFT simulated structural evolution of the system at an initial temperature of 200 K following the photoexcitation using a laser pulse with $E_0 = 0.386$ V/Å. The ultrafast laser pulse excites vertically 50 electrons (or 6% of valence electrons) from the valence bands to the empty conduction bands within 100 fs duration [shown in Fig. 1(c)]. Following the photoexcitation, we find that the Ir-Ir dimers undergo dissociation (at about 100 fs) as their bond length gets longer from 3.07 Å and at 650 fs reaching the maximum (around 4.1 Å), passing through 3.9 Å, the same value as that of nondimer partners. Finally, Ir-Ir dimers and Ir-Ir nondimers exhibit no significant differences in bond length, indicating the system stabilized in the HT structure. Consequently, we have successfully reproduced theoretically the experimentally observed phase transition from LT structure to HT structure of $IrTe_2$ under ultrafast photoexcitation, as reported recently by Ideta *et al.* [23] and Monney *et al.* [27].

We uncover that strong photoexcitation does not necessarily guarantee the system will undergo the LT-to-HT structural transition. To explore the dependence of the phase transition on photoexcitation strength, we tune the laser pulse within a wide span of intensity from 0.051 to 1.02 V/Å. Figure 1(g) shows the corresponding rt-TDDFT simulated dynamics of bond length of the Ir-Ir dimers (once it increases to 3.9 Å, indicating a LT-to-HT phase transition). We observe that the laser intensities can be divided into three ranges according to the atomic bond dynamics. When the laser intensity E_0 is in a weak range from 0.051 to 0.206 V/Å, we notice that the dimerized Ir-Ir bonds vibrate over time in a large amplitude but without completely dissociating. Further increasing the laser intensity (to a range from 0.257 to 0.643 V/Å) [shown in Fig. 1(g)], the bond length of the Ir-Ir dimers increases steadily with time and reaches ∼3.9 Å at about 800 fs, demonstrating a fast dissociation process of the Ir-Ir dimers, hence a successful phase transition. Note that, in the most beginning following the photoexcitation, as amplifying the laser intensity, the increase of the Ir-Ir dimer's bond length is getting slower. It indicates that the breaking of the Ir-Ir dimer bond is not always proportional to the energy pumped into the system. As the laser intensity further increases from 0.643 V/Å to 0.771, 0.900, and 1.028 V/Å, the Ir-Ir dimer bond is no longer dissociated, but vibrates over time in a similar way as in the low laser intensities. This failure to have the LT-to-HT phase transition at stronger laser intensity is rather striking. Such nonmonotonic laser-intensity dependence of the dynamic process is highly unexpected in terms of previously proposed mechanisms [28] for photoinduced phase transitions.

III. DISCUSSION

To inspect the effect of photoelectrons on structural transitions, we first conduct a ground-state Born-Oppenheimer molecular dynamics (BOMD) simulation for $IrTe_2$ neglecting the excitation of electrons. In the BOMD simulation, we find that the dissociation of the Ir-Ir dimers is unlikely to occur, which we attribute to the lack of photoelectron occupation of the empty conduction bands (see Supplemental Material Fig. S1 [29]). Under laser irradiation, a stronger laser intensity always excites more electrons from the valence bands to the empty conduction bands. Figure 1(e) shows that the number of excited electrons scales linearly to the laser intensity when $E_0 < 0.514$ V/Å, whereas it becomes a sublinear scaling when $E_0 > 0.514$ V/Å. The sublinear scaling behavior is due to the band filling effect. According to Fermi's "golden rule," the density of photoexcited electrons making a valence-to-conduction-band transition per time interval is proportional to the density of (initial) electrons occupying the valence bands and to the density of (final) empty conduction-band states. If a significant amount of electrons have been excited from the

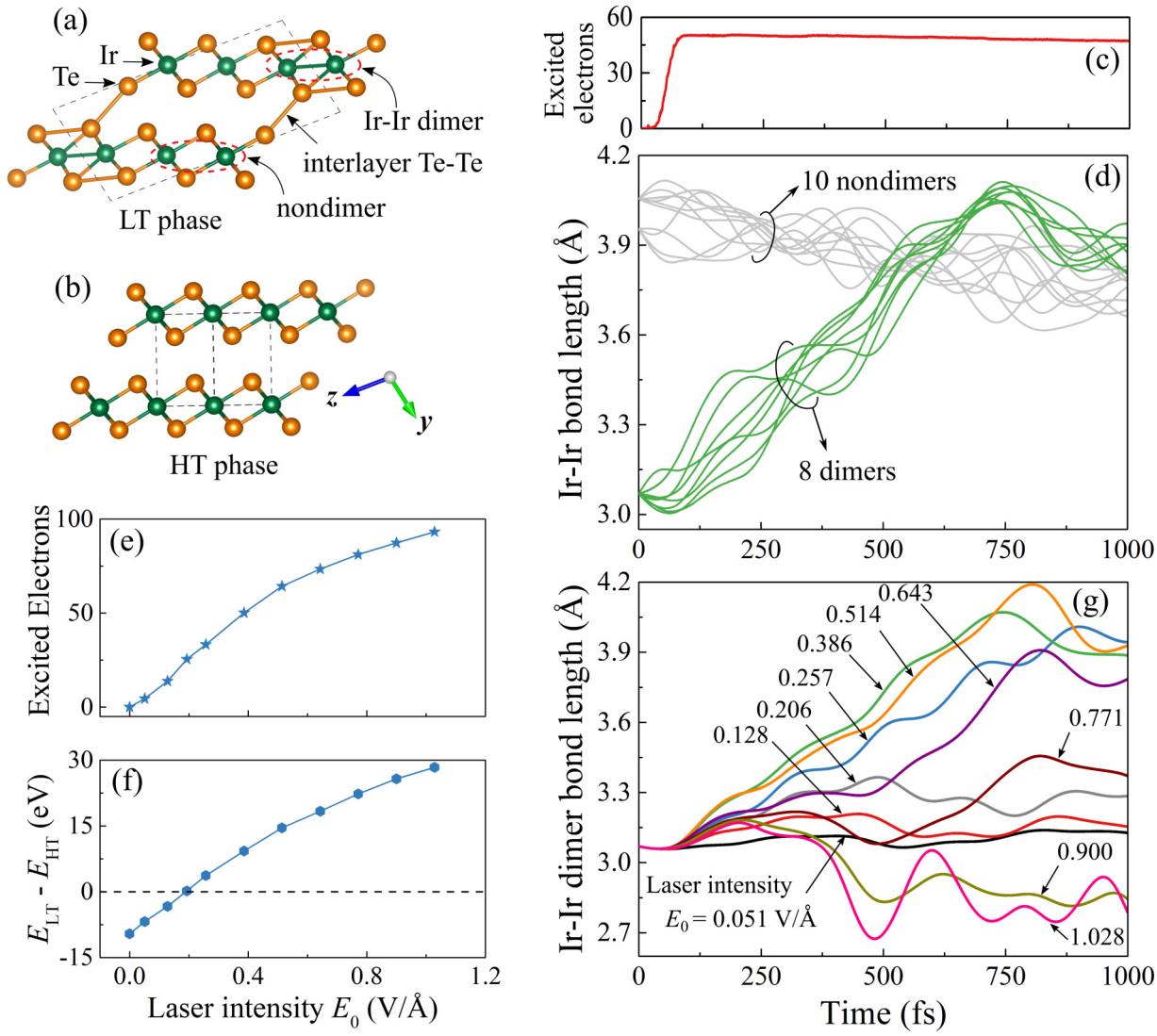

FIG. 1. Structural dynamics of $IrTe_2$ under irradiation of a laser pulse with amplitude (intensity) at $E_0 = 0.386\,\mathrm{V/Å}$. The $IrTe_2$ atomic structure of (a) high-temperature (HT) phase and (b) low-temperature (LT) phase with Ir-Ir dimerized (1/5,0,1/5) lattice modulation. The dashed lines represent the unit cell. (c) The number of photoexcited electrons as a function of time. (d) Dynamic evolution of Ir-Ir bond lengths, including eight pairs of Ir-Ir dimers (green lines) and ten pairs of nondimers (grey lines). (e) The saturation number of photoexcited electrons (ζ) and (f) energy difference between the LT phase and HT phase as a function of laser intensity E_0. (g) The bond evolution of Ir-Ir dimers under irradiation of laser pulses with intensity varying from 0.051 to 1.02 V/Å.

valence bands to the conduction bands, the density of both initial electrons and finial empty states reduces remarkably thus causing a sublinear scaling of excited electrons against laser intensity. We use an occupation constrained DFT (which is to occupy the conduction-band states according to the occupation population obtained from the TDDFT simulations, in a self-consistent DFT calculation) to get the energy difference between the LT phase and HT phase ($\Delta E = E_{\mathrm{LT}} - E_{\mathrm{HT}}$) under different excited states. Figure 1(f) shows that the energy difference increases monotonically from negative to positive following the continuous increment in the laser intensity. All these are in stark contrast to the nonmonotonic behavior in the dimer breaking exhibited in Fig. 1(g). To fully understand this, we have calculated the potential-energy surface (PES) under different laser intensities along a line of different Ir-Ir dimer bond lengths, calculated using the occupation constraint DFT (using TDDFT resulted excitation occupation), as shown in Supplemental Material Fig. S2 [29]. This sheds some light on why at high laser intensity the phase transition does not happen: there is another minimum at even shorter Ir-Ir bond length, which can trap the system. Nevertheless, it is still not clear why at higher laser energy, the PES will have such a change of shape.

Photoelectrons are excited vertically from the valence bands to the empty conduction bands, both consisting of Ir $5d$ orbitals and Te $5p$ orbitals as shown in Fig. 1(c). In the LT phase, the Ir-Ir dimerization forms a covalent bond and the interaction between $5d_{xz}(5d_{yz})$ orbitals of two Ir atoms produces bonding and antibonding bands straddling the Fermi level [Fig. 2(d)]. The energy of the antibonding band is raised from the atomic orbital level over the Fermi energy E_f by an amount V_d (usually referred to as the overlap parame-

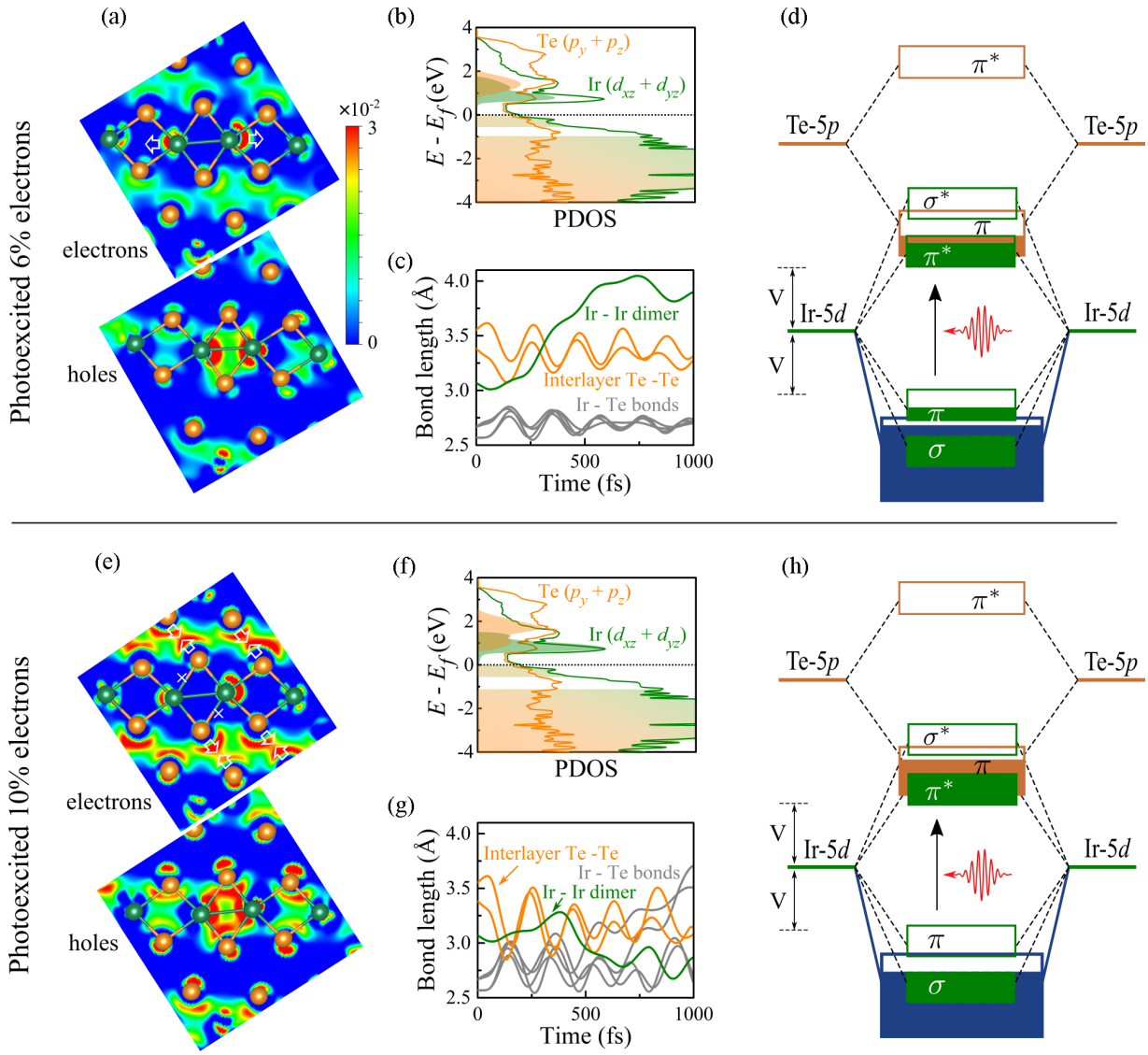

FIG. 2. The microscopic force driving the structural transition arising from photoinduced electron modulation (a)–(d) for the case of photoexcited 6% valence electrons, (e)–(h) for the case of photoexcited 10% valence electrons. (a),(e) Real-space distribution of photoexcited electrons and holes on the $(11\bar{1})$ plane for (a) photoexcitation of 6% electrons and (e) photoexcitation of 10% electrons to empty bands above the Fermi level at the end of the laser pulses (∼120 fs). (b),(f) Partial density of states (PDOS) of the LT phase. Shaded areas represent electronic occupation right following the photoexcitation. (c),(g) Evolution of the atomic structure under photoexcitation, showing the time dynamics of bond lengths of selected bonds which chart the progress of the photoinduced structural transitions. (d),(h) Schematic diagram of the bonding and antibonding bands of intralayer Ir-Ir dimers and interlayer Te-Te bonds. The white hollow arrows in (a) and (e) mark the direction of force driving the atoms away from equilibrium positions. The white cross symbols in (e) indicate the breaking of Ir-Te bonds during structural transition.

ter), the same as the lowering of the bonding band energy [30]. However, due to the bond geometric relationship and the Poisson ratio exhibited by the Ir-Te-Ir-Te parallelogram, the Ir-Ir dimerization will push away the Te atom vertically within that bonded parallelogram, and make the Te form an interlayer Te-Te pair as indicated in Fig. 1(a). The empty Te $5p$ orbitals are higher in energy than Ir $5d$ orbitals; the hybridized Te $5p_y(5p_z)\pi$ bands bond state of the interlayer Te-Te dimers are slightly higher in energy than the antibonding state of the Ir-Ir $5d_{xz}(5d_{yz})\pi^*$ bands, as shown in Fig. 2(d) (see Supplemental Material Fig. S3 for more details [29]). All these are confirmed in the partial density of states [Fig. 2(b)] of the DFT calculation. Note at the ground state, the Te-Te pair should not be called a bond, since their Te $5p_y(5p_z)\pi$ bonding state is not occupied with any electron. A weak laser pulse excites n electrons from the (valence bands) bonding Ir $5d$ π bands of the Ir-Ir dimers to the (conduction bands) antibonding Ir $5d$ π^* bands of the Ir-Ir dimers, raising the system energy in an amount of about $2nV_d$. The real-space charge distribution of photoelectrons and photoexcited holes in the case of $E_0 = 0.386\,\mathrm{V/Å}$ (6% of total valence electrons) is shown in Fig. 2(a). One can see that the photoexcited holes have a finite component within the Ir-Ir dimer center bonding region, whereas photoinduced electrons vanishes in the Ir-Ir dimer center but maximize at its two ends, a characteristic of the antibonding state. The photoexcited system will gain

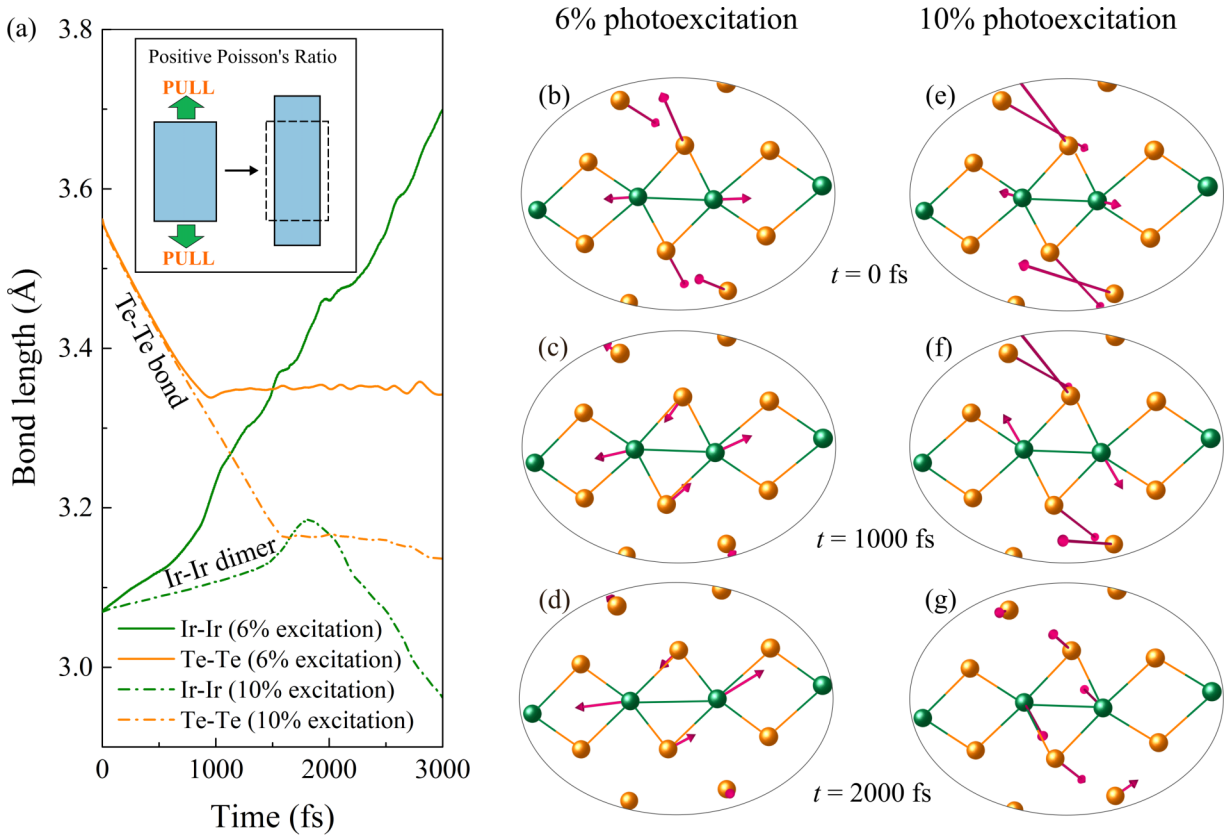

FIG. 3. Evolution of bond length and atomic force in ultrafast dynamics at $T = 1$ K (a) for evolution of Ir-Ir and Te-Te bond length in photoexcited 6% and 10% electrons (the inset shows the schematic diagram of positive poison's ratio in materials), (b)–(d) for the structural snapshots of photoexcited 6% valence electrons, (e)–(g) for the structural snapshots of photoexcited 10% valence electrons, (b)–(d) and (e)–(g) for atomic driving forces at different times. The pink arrows represent direction and magnitude of forces.

energy from both lowering the eigenenergy of excited electrons and raising the eigenenergy of excited holes by reducing V_d through increasing the Ir-Ir bonds length. This causes the PES trend shown in Fig. S2 [29], when the laser intensity is weaker than 0.386 V/Å. As the laser intensity increases, the tendency toward the HT phase also increases, until enough excitation is created, and the HT becomes more stable. Thus, we illustrate that the dissociation of the Ir-Ir dimers are due to the filling of the antibonding state, as well as the emptying of the bonding state, a picture similar to that proposed by Ideta *et al.* [23], although they only emphasized the filling of the antibonding state in their argument.

If the laser pulse intensity is further increased, the photoexcited electrons begins to fill in the bonding bands of Te-Te dimers as shown in Figs. 2(e) and 2(h). In real space, we see that photoexcited electron density localized at the interlayer Te-Te bonds increases remarkably as the excited number of electrons increases from 6% to 10% of total valence band [Fig. 2(e)]. The occupation of the bonding state of the interlayer Te-Te dimers [Fig. 2(h)] tends to reduce the bond length of the interlayer Te-Te dimers (so it will lower the bonding state energy), which in turn also reduces the Ir-Ir dimer distance due to the Poisson ratio of the Ir-Te-Ir-Te parallelogram. This thus acts as a counter force to the tendency to increase the Ir-Ir dimer distance due to the occupation of the Ir-Ir antibond states. As laser intensity further increases, this Te-Te dimer reduction tendency overcomes the Ir-Ir dimer increase tendency, and the structure finds a new energy minimum as shown in Fig. S2 [29]. The competition between these two occupations of different bands and the opposite tendency for bond length changes provide an intriguing picture of how the phase transition happens under different mechanisms. Our analysis also provides a way to understand this complicated phase-transition process.

Lattice vibrations or phonons are usually considered as playing an important role in different phase transitions [24,31,32]. After all, in the temperature induced phase transition, it is the thermal vibration which initiates the phase transition. In the above simulations, we have used 200 K temperature. To eliminate phonon-induced harmonic force on each atom and remove the possible cause by lattice vibrations, we rerun the rt-TDDFT simulations at an extreme low temperature of 1 K. However, to make the analysis easier, instead of using an explicit laser pulse as we did above, we now use an initial excited-state occupation as we obtained from previous rt-TDDFT simulation after the laser pulse duration. Figure 3(a) shows the dynamic evolution of bonds of intralayer Ir-Ir dimer and interlayer Te-Te dimer obtained from low-temperature rt-TDDFT simulations. We find that for 6% photoexcitation the Ir-Ir dimer also undergoes a dissolution at 1 K but in a longer time scale compared with the 200-K case. This result indicates phonons are not essential but nevertheless can assist the photo-induced LT-to-HT phase transitions (phonon modes, Fig. S6 [29]). This is natural since

at high enough temperature, the system will change from LT to HT without laser excitation. We thus can analyze the transition drive into two sources: one is the thermal dynamic source, which has a random disordered transition path, another is the electron excitation source, which has an ordered and deterministic coherent path. Since we are talking about structure phase transition, inevitably, phonon (lattice distortion) is involved, and electron-phonon coupling is essential. But still, we think the thermal phonon is not the driving force since the phase transition happens before the excited electrons have been fully relaxed with their excess energy converted into thermal phonons, and the lattice temperature at the phase-transition point is not that high. Instead, the phonons or lattice vibrations regulate the time scale of phase transition via changing dynamically the energy barrier associated with the structural phase transition. The coherent path can be analyzed by the atomic force in the 1-K low-temperature simulation. Figure 3(b) displays the atomic forces exerting on atoms of the Ir-Ir and Te-Te dimers at $t = 0$. These forces arise completely from the occupation of photoelectrons and photoholes as we explained above. Specifically, photoholes and photoelectrons occupied antibonding and bonding Ir $5d$ bands of the Ir-Ir dimers, respectively, producing a force to stretch the Ir-Ir dimer, whereas photoelectrons occupied bonding bands of the Te-Te dimers, creating a force to contract the Te-Te dimer as the system will lower energy from decreasing the Te-Te dimers distance. The two (almost) vertical forces are in competition through a positive Poisson ratio of the Ir-Te-Ir-Te parallelogram with the Ir-Ir horizontal out-stretching forces as discussed above. As we can see, as the excitation increases from 6% to 10%, the atomic force for the Te atom increases, while that for the Ir atom reduces. The atomic forces evolve in a deterministic fashion with time. But the evolution for 6% and 10% are dramatically different, corroborating with the bond length changes as shown in Fig. 3(a). In the case of 10% excitation, a new structure is reached at the end of the excitation, corresponding to a local minimum of the structure as shown in Fig. S2 [29].

In summary, through the rt-TDDFT simulation, together with occupation constraint DFT calculations, we have revealed the intriguing dynamics in the laser pulse induced phase change in the $IrTe_2$ crystal. The central insight is that the photoexcited carriers can occupy different states. When the antibonding state is occupied, it will increase the corresponding bond length. On the other hand, if a higher energy bonding state is occupied, it can reduce the bond length of that atomic pair. Besides analyzing the excitation in energy spectrum, filling bonding and antibonding states, one can also analyze the case in real space, by plotting the excited electron and hole localization. One can see, clearly occupying the bond location at the center of an atom pair will tend to reduce the atom pair distance, while occupying the antibonding location (at the two ends of the atom pair) will tend to enlarge the atom distance, as these show up in the atomic force plot. Furthermore, due to bonding geometry and connection (and their Poisson ratio), different driving forces can work together, or against each other. We also demonstrated that phonons, usually proposed as the critical factors, are inessential but can assist the photoinduced phase transitions. All these show that the laser induced phase transition can have complicated behavior more than the ground-state dynamics. Understanding the underlying mechanism can also help us to design new excitations to initiate different phase-transition behavior and thus enable more explicit material manipulations.

ACKNOWLEDGMENTS

The work in China was supported by the Key Research Program of Frontier Sciences, CAS under Grant No. ZDBS-LY-JSC019, and the National Natural Science Foundation of China (NSFC) under Grant No. 11925407. L.W.W. was supported by the Director, Office of Science (SC), Basic Energy Science (BES), Materials Science and Engineering Division (MSED), of the US Department of Energy (DOE) under Contract No. DE-AC02-05CH11231 through the Materials Theory program (KC2301).

[1] V. R. Morrison, R. P. Chatelain, K. L. Tiwari, A. Hendaoui, A. Bruhacs, M. Chaker, and B. J. Siwick, A photoinduced metal-like phase of monoclinic VO_2 revealed by ultrafast electron diffraction, Science **346**, 445 (2014).

[2] S. Gerber, S. L. Yang, D. Zhu, H. Soifer, J. A. Sobota, S. Rebec, J. J. Lee, T. Jia, B. Moritz, C. Jia, A. Gauthier, Y. Li, D. Leuenberger, Y. Zhang, L. Chaix, W. Li, H. Jang, J. S. Lee, M. Yi, G. L. Dakovski *et al.*, Femtosecond electron-phonon lock-in by photoemission and x-ray free-electron laser, Science **357**, 71 (2017).

[3] M. Buzzi, M. Först, R. Mankowsky, and A. Cavalleri, Probing dynamics in quantum materials with femtosecond x-rays, Nat. Rev. Mater. **3**, 299 (2018).

[4] H. Oike, M. Kamitani, Y. Tokura, and F. Kagawa, Kinetic approach to superconductivity hidden behind a competing order, Sci. Adv. **4**, eaau3489 (2018).

[5] K. Okazaki, Y. Ogawa, T. Suzuki, T. Yamamoto, T. Someya, S. Michimae, M. Watanabe, Y. Lu, M. Nohara, H. Takagi, N. Katayama, H. Sawa, M. Fujisawa, T. Kanai, N. Ishii, J. Itatani, T. Mizokawa, and S. Shin, Photo-induced semimetallic states realised in electron-hole coupled insulators, Nat. Commun. **9**, 4322 (2018).

[6] S. Wall, S. Yang, L. Vidas, M. Chollet, J. M. Glownia, M. Kozina, T. Katayama, T. Henighan, M. Jiang, T. A. Miller, D. A. Reis, L. A. Boatner, O. Delaire, and M. Trigo, Ultrafast disordering of vanadium dimers in photoexcited VO_2, Science **362**, 572 (2018).

[7] M. R. Otto, L. P. Rene de Cotret, D. A. Valverde-Chavez, K. L. Tiwari, N. Emond, M. Chaker, D. G. Cooke, and B. J. Siwick, How optical excitation controls the structure and properties of vanadium dioxide, Proc. Natl. Acad. Sci. USA **116**, 450 (2019).

[8] M. Eichberger, H. Schafer, M. Krumova, M. Beyer, J. Demsar, H. Berger, G. Moriena, G. Sciaini, and R. J. Miller, Snapshots of cooperative atomic motions in the optical suppression of charge density waves, Nature (London) **468**, 799 (2010).

[9] T. Rohwer, S. Hellmann, M. Wiesenmayer, C. Sohrt, A. Stange, B. Slomski, A. Carr, Y. Liu, L. M. Avila, M. Kallane, S. Mathias, L. Kipp, K. Rossnagel, and M. Bauer, Collapse of long-range charge order tracked by time-resolved photoemission at high momenta, Nature (London) **471**, 490 (2011).

[10] A. Zong, A. Kogar, Y.-Q. Bie, T. Rohwer, C. Lee, E. Baldini, E. Ergeçen, M. B. Yilmaz, B. Freelon, E. J. Sie, H. Zhou, J. Straquadine, P. Walmsley, P. E. Dolgirev, A. V. Rozhkov, I. R. Fisher, P. Jarillo-Herrero, B. V. Fine, and N. Gedik, Evidence for topological defects in a photoinduced phase transition, Nat. Phys. **15**, 27 (2018).

[11] A. Kogar, A. Zong, P. E. Dolgirev, X. Shen, J. Straquadine, Y.-Q. Bie, X. Wang, T. Rohwer, I. C. Tung, Y. Yang, R. Li, J. Yang, S. Weathersby, S. Park, M. E. Kozina, E. J. Sie, H. Wen, P. Jarillo-Herrero, I. R. Fisher, X. Wang, and N. Gedik, Light-induced charge density wave in $LaTe_3$, Nat. Phys. **16**, 159 (2019).

[12] A. Zong, P. E. Dolgirev, A. Kogar, E. Ergecen, M. B. Yilmaz, Y. Q. Bie, T. Rohwer, I. Cheng Tung, J. Straquadine, X. Wang, Y. Yang, X. Shen, R. Li, J. Yang, S. Park, M. C. Hoffmann, B. K. Ofori-Okai, M. E. Kozina, H. Wen, X. Wang, I. R. Fisher, P. Jarillo-Herrero, and N. Gedik, Dynamical Slowing-Down in an Ultrafast Photoinduced Phase Transition, Phys. Rev. Lett. **123**, 097601 (2019).

[13] T. Toriyama, M. Kobori, T. Konishi, Y. Ohta, K. Sugimoto, J. Kim, A. Fujiwara, S. Pyon, K. Kudo, and M. Nohara, Switching of conducting planes by partial dimer formation in $IrTe_2$, J. Phys. Soc. Jpn. **83**, 033701 (2014).

[14] G. L. Pascut, K. Haule, M. J. Gutmann, S. A. Barnett, A. Bombardi, S. Artyukhin, T. Birol, D. Vanderbilt, J. J. Yang, S. W. Cheong, and V. Kiryukhin, Dimerization-Induced Cross-Layer Quasi-Two-Dimensionality in Metallic $IrTe_2$, Phys. Rev. Lett. **112**, 086402 (2014).

[15] D. Ootsuki, S. Pyon, K. Kudo, M. Nohara, M. Horio, T. Yoshida, A. Fujimori, M. Arita, H. Anzai, H. Namatame, M. Taniguchi, N. L. Saini, and T. Mizokawa, Electronic structure reconstruction by orbital symmetry breaking in $IrTe_2$, J. Phys. Soc. Jpn. **82**, 093704 (2013).

[16] K. Kim, S. Kim, K. T. Ko, H. Lee, J. H. Park, J. J. Yang, S. W. Cheong, and B. I. Min, Origin of First-Order-Type Electronic and Structural Transitions in $IrTe_2$, Phys. Rev. Lett. **114**, 136401(2015).

[17] H. Cao, B. C. Chakoumakos, X. Chen, J. Yan, M. A. McGuire, H. Yang, R. Custelcean, H. Zhou, D. J. Singh, and D. Mandrus, Origin of the phase transition in $IrTe_2$: structural modulation and local bonding instability, Phys. Rev. B **88**, 115122 (2013).

[18] J. J. Yang, Y. J. Choi, Y. S. Oh, A. Hogan, Y. Horibe, K. Kim, B. I. Min, and S. W. Cheong, Charge-Orbital Density Wave and Superconductivity in the Strong Spin-Orbit Coupled $IrTe_2$:Pd, Phys. Rev. Lett. **108**, 116402 (2012).

[19] D. Ootsuki, Y. Wakisaka, S. Pyon, K. Kudo, M. Nohara, M. Arita, H. Anzai, H. Namatame, M. Taniguchi, N. L. Saini, and T. Mizokawa, Orbital degeneracy and peierls instability in the triangular-lattice superconductor $Ir_{1-x}Pt_xTe_2$, Phys. Rev. B **86**, 014519 (2012).

[20] A. F. Fang, G. Xu, T. Dong, P. Zheng, and N. L. Wang, Structural phase transition in $IrTe_2$: a combined study of optical spectroscopy and band structure calculations, Sci. Rep. **3**, 1153 (2013).

[21] Q. Li, W. Lin, J. Yan, X. Chen, A. G. Gianfrancesco, D. J. Singh, D. Mandrus, S. V. Kalinin, and M. Pan, Bond Competition and phase evolution on the $IrTe_2$ surface, Nat. Commun. **5**, 5358 (2014).

[22] D. Mazumdar, K. Haule, J. J. Yang, G. L. Pascut, B. S. Holinsworth, K. R. O'Neal, V. Kiryukhin, S.-W. Cheong, and J. L. Musfeldt, Optical evidence for bonding-antibonding splitting in $IrTe_2$, Phys. Rev. B **91**, 041105(R) (2015).

[23] S. I. Ideta, D. Zhang, A. G. Dijkstra, S. Artyukhin, S. Keskin, R. Cingolani, T. Shimojima, K. Ishizaka, H. Ishii, K. Kudo, M. Nohara, and R. J. D. Miller, Ultrafast dissolution and creation of bonds in $IrTe_2$ induced by photodoping, Sci. Adv. **4**, eaar3867 (2018).

[24] N. K. Chen, X. B. Li, J. Bang, X. P. Wang, D. Han, D. West, S. Zhang, and H. B. Sun, Directional Forces by Momentumless Excitation and Order-to-Order Transition in Peierls-Distorted Solids: The Case of GeTe, Phys. Rev. Lett. **120**, 185701 (2018).

[25] J. Zhang, C. Lian, M. Guan, W. Ma, H. Fu, H. Guo, and S. Meng, Photoexcitation induced quantum dynamics of charge density wave and emergence of a collective mode in 1T-TaS_2, Nano Lett. **19**, 6027 (2019).

[26] Y. S. Oh, J. J. Yang, Y. Horibe, and S. W. Cheong, Anionic Depolymerization Transition in $IrTe_2$, Phys. Rev. Lett. **110**, 127209 (2013).

[27] C. Monney, A. Schuler, T. Jaouen, M. L. Mottas, T. Wolf, M. Merz, M. Muntwiler, L. Castiglioni, P. Aebi, F. Weber, and M. Hengsberger, Robustness of the charge-ordered phases in $IrTe_2$ against photoexcitation, Phys. Rev. B **97**, 075110 (2018).

[28] B. Peng, H. Zhang, W. Chen, B. Hou, Z.-J. Qiu, H. Shao, H. Zhu, B. Monserrat, D. Fu, H. Weng, and C. M. Soukoulis, Sub-Picosecond photo-induced displacive phase transition in two-dimensional $MoTe_2$, npj 2D Mater. Appl. **4**, 14 (2020).

[29] See Supplemental Material at http://link.aps.org/supplemental/10.1103/PhysRevB.102.184308 for methods and supplemental results, which include Refs. [14,16,23,33–37].

[30] W. A. Harrison, *Elementary Electronic Structure* (World Scientific, Singapore, 1999), Chap. 5.

[31] G. Sciaini, M. Harb, S. G. Kruglik, T. Payer, C. T. Hebeisen, F. J. zu Heringdorf, M. Yamaguchi, M. Horn-von Hoegen, R. Ernstorfer, and R. J. Miller, Electronic acceleration of atomic motions and disordering in bismuth, Nature (London) **458**, 56 (2009).

[32] L. Rettig, S. O. Mariager, A. Ferrer, S. Grubel, J. A. Johnson, J. Rittmann, T. Wolf, S. L. Johnson, G. Ingold, P. Beaud, and U. Staub, Ultrafast Structural Dynamics of the Fe-Pnictide Parent Compound $BaFe_2As_2$, Phys. Rev. Lett. **114**, 067402 (2015).

[33] Z. Wang, S. S. Li, and L. W. Wang, Efficient Real-Time Time-Dependent Density Functional Theory Method and Its Application to a Collision of an Ion with a 2d Material, Phys. Rev. Lett. **114**, 063004 (2015).

[34] D. R. Hamann, Optimized norm-conserving vanderbilt pseudopotentials, Phys. Rev. B **88**, 085117 (2013).

[35] W. L. Jia, Z. Y. Cao, L. Wang, J. Y. Fu, X. B. Chi, W. G. Gao, and L. W. Wang, The analysis of a plane wave pseudopotential density functional theory code on a gpu machine computer, Phys. Commun. **184**, 9 (2013).

[36] N. Lazarevic, E. S. Bozin, M. Scepanovic, M. Opacic, H. C. Lei, C. Petrovic, and Z. V. Popovic, Probing $IrTe_2$ crystal symmetry by polarized raman scattering, Phys. Rev. B **89**, 224301 (2014).

[37] A. Glamazda, K. Y. Choi, P. Lemmens, J. J. Yang, and S. W. Cheong, Proximity to a commensurate charge modulation in $IrTe_{2-x}Se_x$ ($x = 0$ and 0.45) revealed by raman spectroscopy, New J. Phys. **16**, 093061 (2014).